2010-01-01

Simulation Algorithm and Validation of a Photovoltaic Water Pumping System

I. Odeh
Ammann, Jordan

Y. Yohannis
University of Ulster

Brian Norton
Technological University Dublin, brian.norton@tudublin.ie

Recommended Citation

Odeh, Y.G. Yohanis & Norton, B. (2010). Simulation Algorithm and Validation of a Photovoltaic Water Pumping System. *Proceedings of the Institution of Mechanical Engineers, Part A Journal of Energy and Power*, vol. 224, no.10,pp.641-656. doi:10.1243/09576509JPE843

Simulation algorithm and validation of a photovoltaic water pumping system model using long-term field data

I Odeh[1], **Y G Yohanis**[2*], and **B Norton**[3]
[1]Sweileh, Amman, Jordan
[2]Centre for Sustainable Technologies, University of Ulster, Newtownabbey, UK
[3]Dublin Energy Laboratory, Dublin Institute of Technology, Dublin, Ireland

The manuscript was received on 19 June 2009 and was accepted after revision for publication on 18 February 2010.

DOI: 10.1243/09576509JPE843

Abstract: A photovoltaic (PV) water pumping system has been modelled using TRNSYS considering a power supply, a direct current (DC)/alternating current (AC) inverter, an AC induction motor, a centrifugal pump, a well, a water storage tank, and an overflow protection device. The model emulates actual pumping head curves, uses numerical methods to determine pump-system working points, and includes a storage tank as a component in the system. It simulates PV-powered water pumping systems, constant voltage tracking, voltage frequency modulation, and maximum power point tracking algorithms; variable inverter frequency with variable motor efficiency, variable inverter frequency with constant motor efficiency, and constant inverter frequency with variable motor efficiency algorithms. It also has the facility to calculate the accumulated unused part of the PV energy owing to the pump reaching its maximum capacity limit. Model validation was accomplished by comparing simulated results with both the laboratory measurements and long-term field data from Jordan; good match and accuracy have been achieved.

Keywords: TRNSYS, solar water pumping, desalination

1 INTRODUCTION

The use of photovoltaics (PV) to power water pumps is widespread. It is often more viable than grid extension and avoids the volatility of costs together with uncertainty of supply associated with the provision of diesel fuel to remote diesel-powered pumps [**1**, **2**]. There are many existing software design tools for PV water pumping systems [**3**]. The influence of pumping head, insolation, and PV array size on the performance of PV water pumping systems and their economic viability have been investigated and reported previously [**2**]. Abdolzadeh *et al.* [**4**] investigated the possibility of improving the performance of a PV water pumping system and have shown that when the operating head is fixed, the calculated array power should not be more than the power of the motor pump at maximum speed, because the array and system efficiencies decrease and the remaining array power is not used. The investigation by Vilela and Fraidenraich [**5**] of the relationship between water pumping capacity, storage tank size, and water demand for a given water deficit has shown that these systems yield iso-deficit lines (curves of equal water deficit) if their critical levels (radiation at which pumping begins). These iso-deficit lines allow the calculation of water pumping systems for meeting specified demands. Similar other design tools [**6**, **7**] and a system of design based on experimental work have been proposed [**8**, **9**]. A similar tool that can consider rapid performance variations of a PV pumping system has also been developed [**10**].

This paper describes the development and validation of a model that uses actual pumping head and a 'finite volume' storage tank for simulating PV-powered water pumping systems, including the following: constant voltage tracking, voltage frequency modulation, and maximum power point tracking algorithms and variable inverter frequency with variable motor efficiency, variable inverter frequency with constant motor efficiency, and constant inverter frequency with variable motor efficiency algorithms.

*Corresponding author: Centre for Sustainable Technologies, School of the Built Environment, University of Ulster, Shore Road, Jordanstown, Newtownabbey, Northern Ireland BT37 0QB, UK.
email: yg.yohanis@ulster.ac.uk*

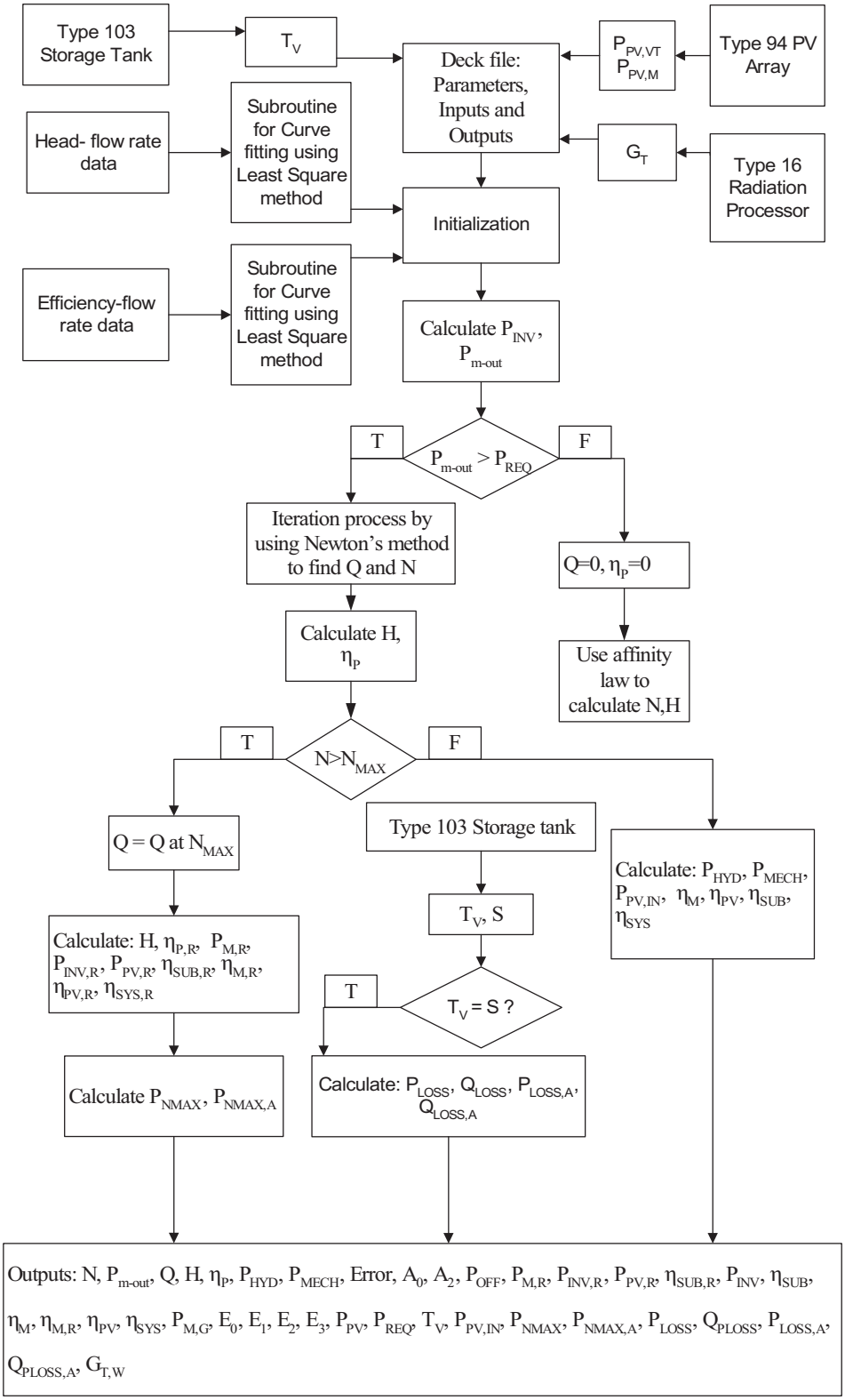

Fig. 1 Component Type 101 Water Pumping Subsystem simulation flow chart

2 METHODOLOGY

PV water pumping system components have been modelled using TRNSYS [**11**]. The system considered consists of the following:

(a) a power supply;
(b) a direct current (DC)/alternating current (AC) inverter;
(c) an AC induction motor;
(d) a centrifugal pump;

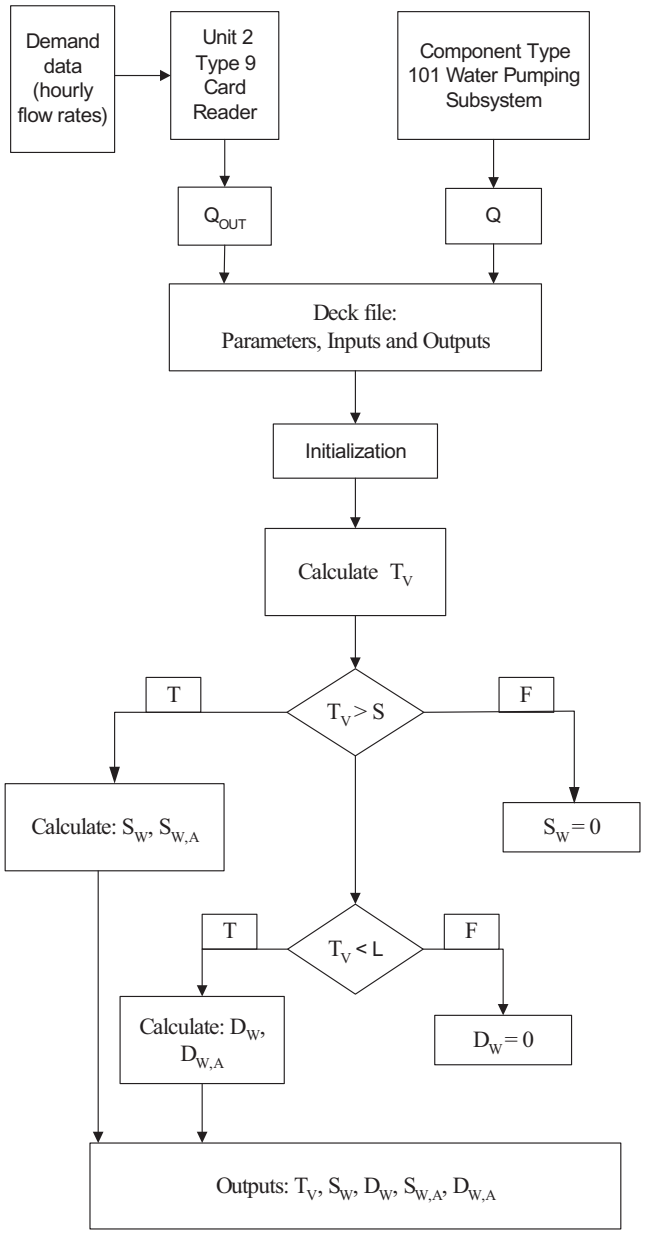

Fig. 2 Component Type 103 Water Storage Tank simulation flow chart

(e) a well;
(f) a water storage tank;
(g) an overflow protection device;
(h) a water desalination system.

TRNSYS [**11**, **12**] was used in modelling to:

(a) enable all simulation options to be undertaken;
(b) consider transient and steady-state conditions;
(c) to easily update the simulation program for any further system development.

TRNSYS's modular structure enables the user to use components available in its library or to program and add newly developed components. Each component has been modelled separately and interconnected

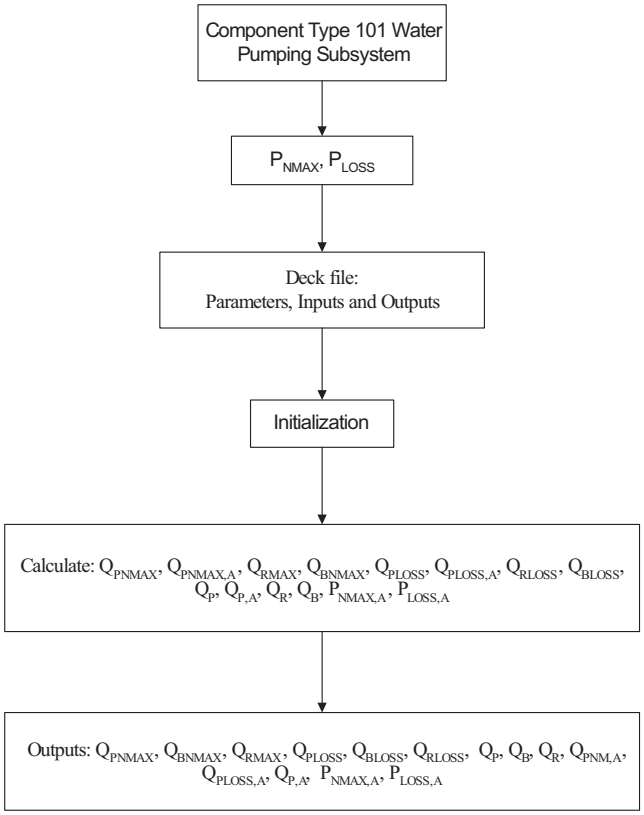

Fig. 3 Component Type 104 Water Desalination Unit simulation flow chart

with other components of the system via a series of inputs and outputs. The model simulates water pumping and water desalination systems powered by PV via a DC/AC inverter. Based on the DC control algorithm of the inverter used, the model simulates constant voltage tracking, voltage frequency modulation, and maximum power point tracking algorithms. For the AC control algorithm of the inverter used, the model simulates 'variable inverter frequency with variable motor efficiency', 'variable inverter frequency with constant motor efficiency', and 'constant inverter frequency with variable motor efficiency' algorithms. The model also simulates grid-connected and diesel-powered water pumping and water desalination systems. Systems coupled with a variable speed drive can also be simulated.

In TRNSYS, a standard component, generally, consists of fixed parameters, variable inputs (that could be outputs of other components), and a group of outputs. A system is structured using a set of components interconnected in such a manner to execute a specific task programmed. A 'deck file' is prepared in which all components' parameters are entered and controlled during the simulation. The deck file also manages inputs and outputs of each component. In this work, Component Type 94 'PV array' available in the TRNSYS library was modified to include a newly developed correlation for PV cell temperature and to simulate different types of inverter algorithms [**13**].

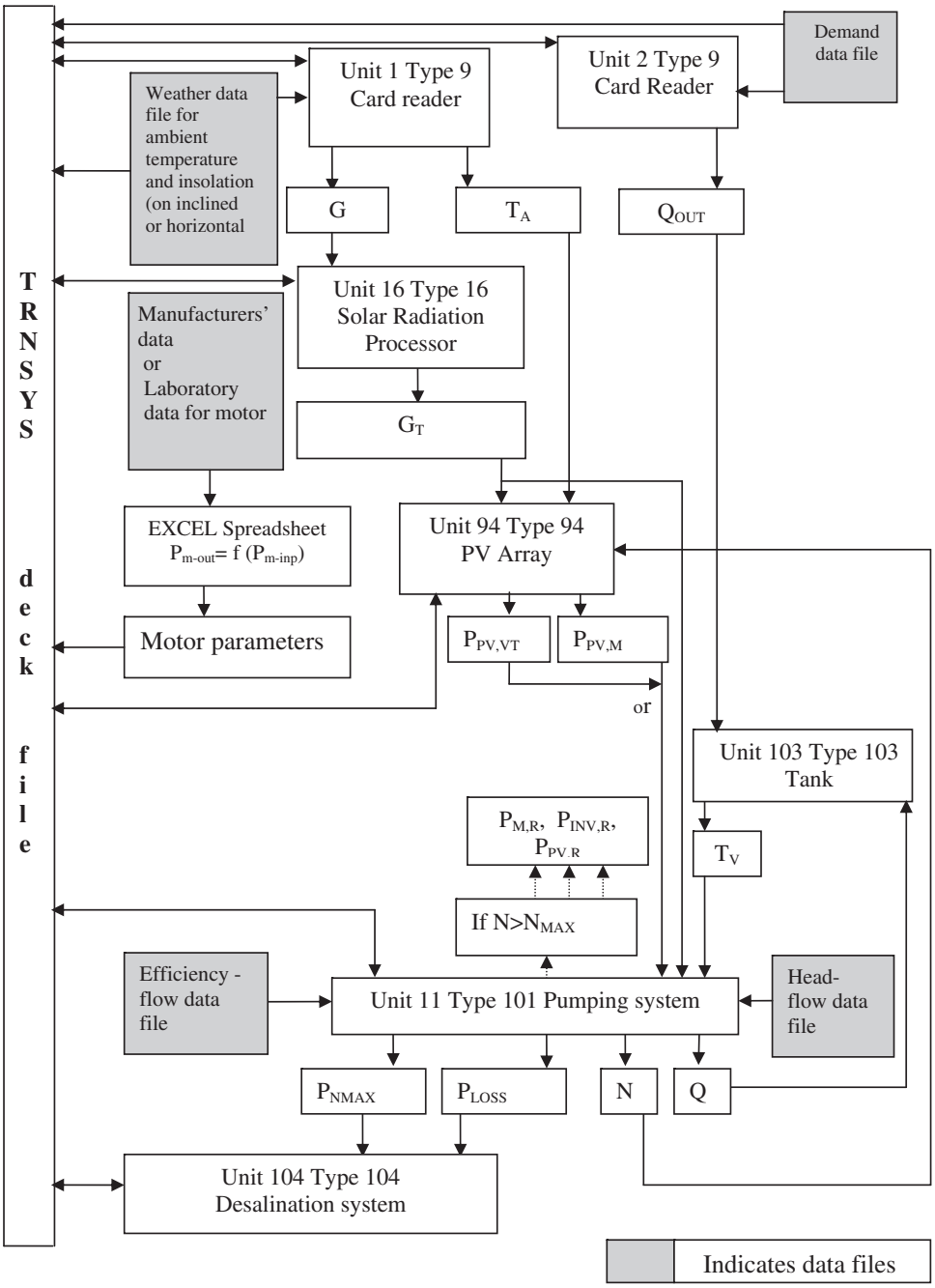

Fig. 4 System components simulation flow diagram

Component Type 9 'Card Reader', Component Type 25 'Printer', Component Type 26 'Plotter', and Component Type 16 'Solar Radiation Processor' were also used from the TRNSYS library. Newly developed components were Type 101 'Water Pumping Subsystem', Component Type 103 'Water Storage Tank', and Component Type 104 'Water Desalination Unit'. Simulation algorithms of Component Types 101, 103, and 104 are illustrated in Figs 1 to 3, respectively. Their inputs and outputs are discussed in Odeh *et al.* [**14**].

A TRNSYS deck file was developed to control the simulation of all components. The model in total had 44 parameters and 19 inputs entered to the deck file, and 65 outputs resulted from the simulation process.

3 SIMULATION

The flow diagram shown in Fig. 4 presents a general description of the model and the components used. The diagram shows only the components, the inputs, and the outputs that are used between the components. Component Type 101 Water Pumping Subsystem simulates the performance of inverter, motor, and pump, given inputs from other

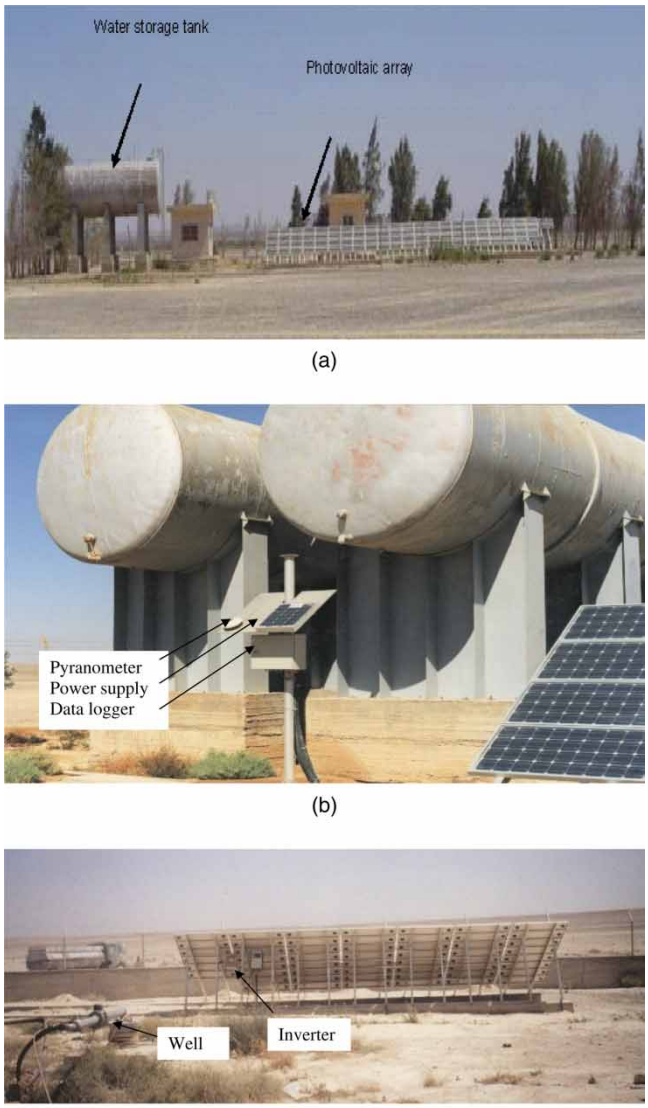

Fig. 5 (a) Ritem PV water pumping system in Jordan; (b) installed data logger; and (c) well and inverter in the Ritem system

components and certain fixed parameters from the deck file. Insolation data on the horizontal plane are processed by Component Type 16 'Radiation Processor' to make the data available to Component Type 94 PV array. If insolation at the plane of the PV array is available, then it can be used by the Component Type 94 via Component Type 9 Card Reader. In-plane insolation and ambient temperature data together with other parameters are used by Component Type 94 to give PV power. Considering the type of the inverter to be used in the PV water pumping system, the output PV power can be either a maximum power point value or a voltage tracking power. The latter can be either of fixed voltage tracking or of voltage frequency modulation output as determined by the inverter employed.

Table 1 Specifications of the M50S PV module [**7**]

Description	Specification
Manufacturer	Siemens Solar
Type	M50S
Base material of cells	Monocrystalline
Maximum power rating (W_p)	50
Rated current (A)	2.9
Rated voltage (V)	17.24
Short circuit current (A)	3.1
Open circuit voltage (V)	21.8
Short circuit current temperature coefficient (%/K)	+0.04
Open circuit voltage temperature coefficient (%/K)	−0.34
Nominal operating cell temperature (°C)	45
No. of cells	36
Length of module (mm)	980
Width of module (mm)	460
Depth of module (mm)	55
Area of module (m^2)	0.4508
Area of cells in the module (m^2)	0.36
Module weight (kg)	7.6
Cell efficiency at standard test conditions (STCs) (%)	13.89
Module efficiency at STCs (%)	11.09

Table 2 Specifications of the Simovert-P-Solar inverter [**8**]

Description	Specification
Manufacturer	Siemens Solar
Type	Simovert-P-Solar
Input voltage range (DC) (V)	135–300
Maximum input voltage (DC) (V)	380
Maximum input short circuit current (DC) (A)	13.3
Apparent power (kVA)	3.5
Peak inverter power for 1 min (kW)	5.2
Load power factor	$\leqslant$0.9 inductive
Rated output current (AC) (A)	9.2
Rated output power for induction motor	2.2 kW, three phase
System voltage	220/240 V±10%
System power factor	$\geqslant$0.95
Output voltage range (AC) (V)	40–240
Output frequency (Hz)	1–100
System frequency (Hz)	50/60
Environmental temperature range (°C)	0–40
Weight (kg)	15

Parameters are used in the deck file to distinguish between the different types of inverters as follows.

1. Parameter number 20 'INVMODE' is used to indicate the voltage tracking algorithm applied in the system, such that INVMODE = 1 is for constant voltage tracking and INVMODE = 2 is for voltage/frequency modulation. The voltage in voltage/frequency modulation inverters is defined by [**11**]

$$V_{\text{inv}} = V_0 + V_1 f \tag{1}$$

where V_0 and V_1 are constants and f is the working frequency of the system. Typically, these inverters are of parameterized type, where the user can set the parameters V_0 and V_1 in the field.

Table 3 Measuring devices and their approximate errors

Parameter	Device	Error
Insolation	CM11 pyranometer [**12**]	±3%
PV voltage	Voltage divider	±0.5%
PV current	Shunt resistance	±0.5%
Flowrate	Counter with Reed-contact	±1% at >0.1 m^3/h ±5% at <0.1 m^3/h
Water level in the well	Pressure sensor (GE Druck)	±1%
Ambient temperature	Thermo resistance PT100	±1 °C
PV cell temperature	Thermo resistance PT100	±1 °C
Wind speed	Anemometer	±2%

Table 4 Data loggers general specifications

	Specification
Hardware	Single-board computer for plug-in memory and modem operation, scalar and vector mean value formation Plug-in module with pre-amplifier and distributing amplifier Three-stage surge – voltage protection for all channels Grid, battery, and solar module operation Desktop and weatherproof housing, temperature range: −25 to +55 °C, tested by TUEV Rhineland
Equipment software	Flash memory for parameter and user programs, enabling easy alteration through evaluation computer Free mathematical coupling of measurement and calculation channels in sampling and mean value formation interval
Initialization and evaluation software	Data transfer at 57 kBaud Setting for secure file systems, overview of availability of data, and editing function Data readout by means of screen, printer, or ASCII files Colour graphics up to four curves simultaneously with variable axis and time axis, backwards and forwards paging of graphic displays

2. Parameter number 21 is the V_0 coefficient of equation (1).
3. Parameter number 22 is the V_1 coefficient of equation (2).

When the voltage frequency modulation algorithm is selected, the system frequency obtained from Component Type 101 is used as input to Component Type 94, where an iterative internal loop is implemented between Component Type 101 and Component Type 94 to find the concerned voltage of the inverter. Inverter output power is determined using the following equation

$$P_{\text{inv}} = \eta_{\text{inv}} P_{\text{pv}} \tag{2}$$

Motor output power is calculated on the basis of the type of the power supply used. For constant motor efficiency algorithm, the following equation is used

$$P_{m-\text{out}} = \eta_m P_{m-\text{inp}} \tag{3}$$

whereas, for variable motor efficiency algorithm, the following equation is used

$$P_{m-\text{out}} = m_0 + m_1 P_{m-\text{inp}} + m_2 P_{m-\text{inp}}^2 \tag{4}$$

The coefficient of this equation, which can be obtained experimentally in the laboratory or from manufacturers' data sheets, is used as parameters for Component Type 101 as the following:

(a) parameter number 11 'm_0' is the zero-order coefficient;
(b) parameter number 12 'm_1' is the first-order coefficient;
(c) parameter number 13 'm_2' is the second-order coefficient.

Head–flowrate (H–Q) data and efficiency–flowrate (η–Q) data of the pump are needed as data files, where

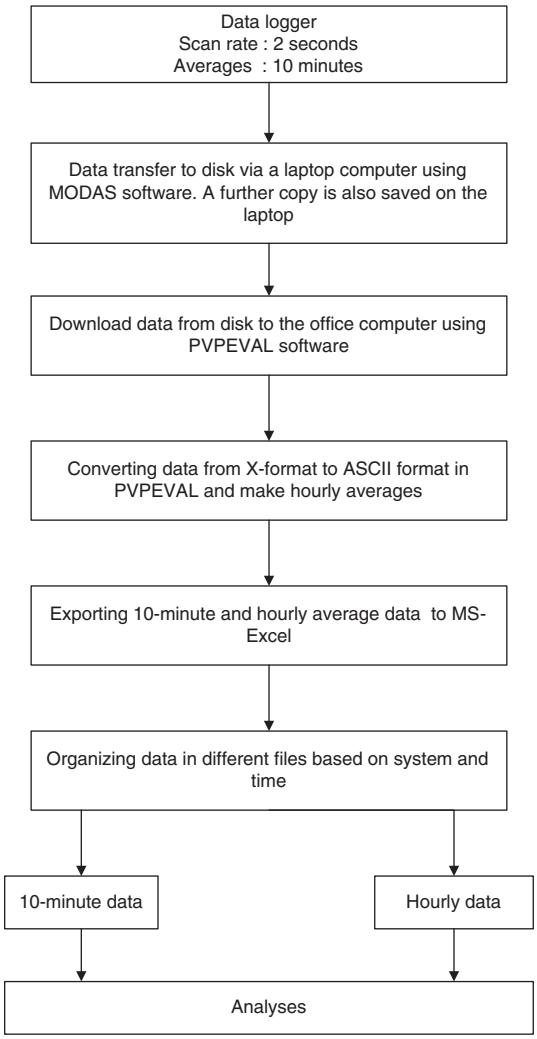

Fig. 6 Data handling process

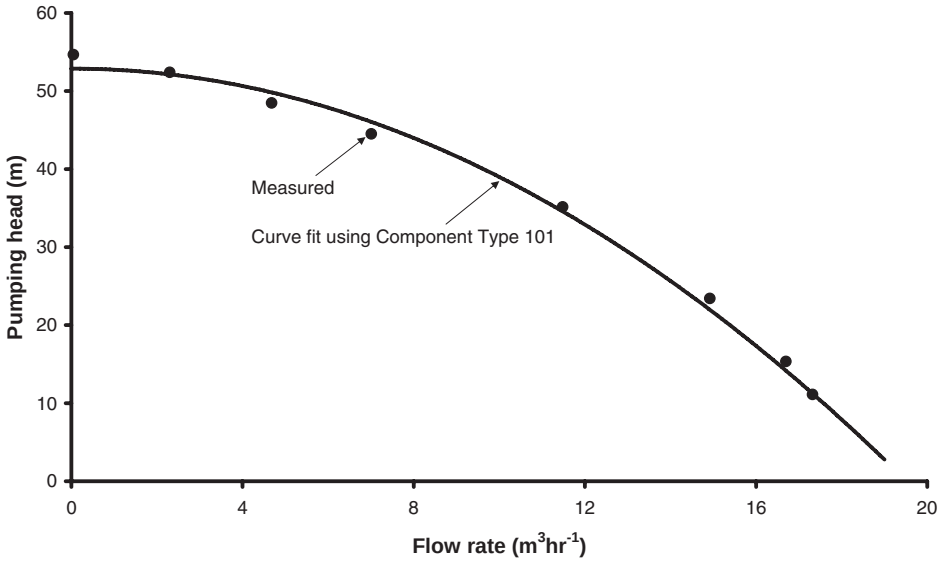

Fig. 7 Measurements and results of the pumping head as a function of flowrate for 50 Hz frequency

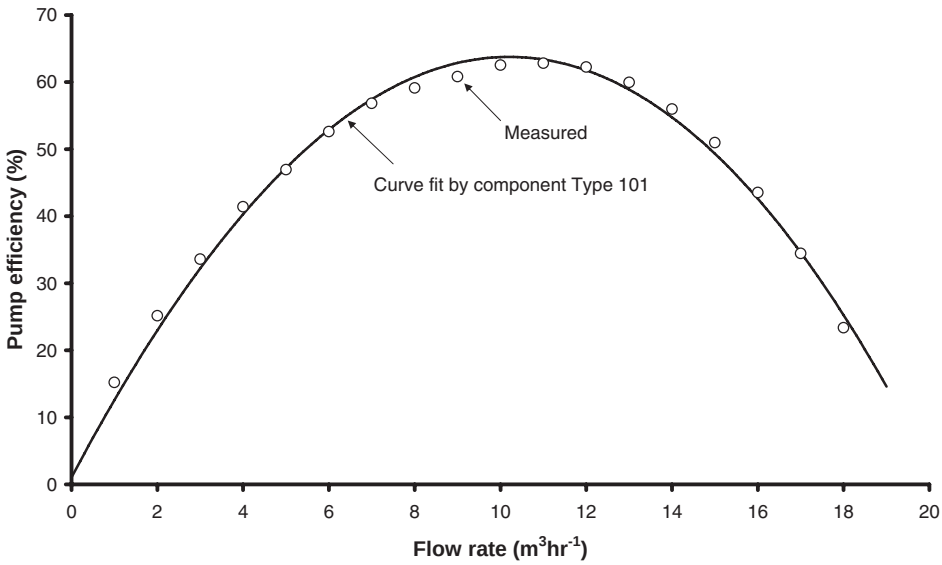

Fig. 8 Measurements and curve-fitting results for pump efficiency as a function of flowrate at 50 Hz

a least-square method is used in Component Type 101 to generate the H–Q data.

The characteristic curves for the pump and the well system are shown in the companion paper by Odeh *et al.* [**14**]. When the pump speed is less than or equal to the maximum speed, determined by the user (parameter number 4 in Component Type 101), the model calculates PV array power, inverter power, motor power, hydraulic power, PV efficiency, motor efficiency, pump efficiency, subsystem efficiency, and system efficiency. When the system speed exceeds the maximum predefined system speed, a constant flowrate (equal to the flowrate at maximum speed) is maintained even when higher insolation is available and all system outputs are recalculated. The model also determines the instantaneous and the accumulated unused part of the PV power (i.e. the difference between available PV power and used PV power). Component Type 103 receives instantaneous system output flowrates from Component Type 101 (output number 3) and instantaneous demand flowrates from a demand data file via Component Type 9 Card Reader. It then determines the instantaneous water volume in the tank (output number 1). Component Type 101 recognizes whether the storage tank is full or not, based on the water volume in the tank (output number 1 in Component Type 103) and the storage tank size (parameter number 9 in Component Type 101). For the periods at which the water storage tank is full, the model (Component Type 101) assumes that the pump was turned off and calculates PV power, flowrate, accumulated PV power, and accumulated flowrate, assuming

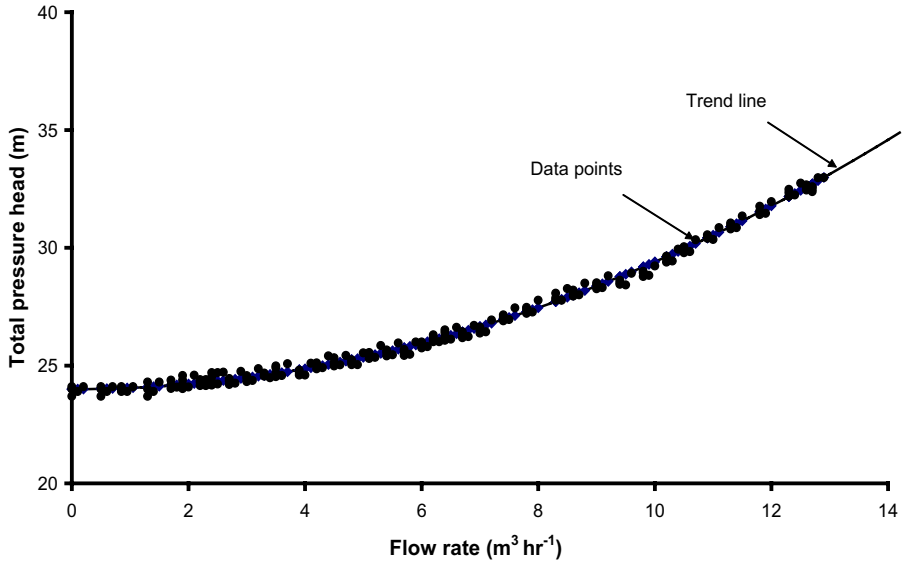

Fig. 9 Measurements of well system pumping head as a function of flowrate

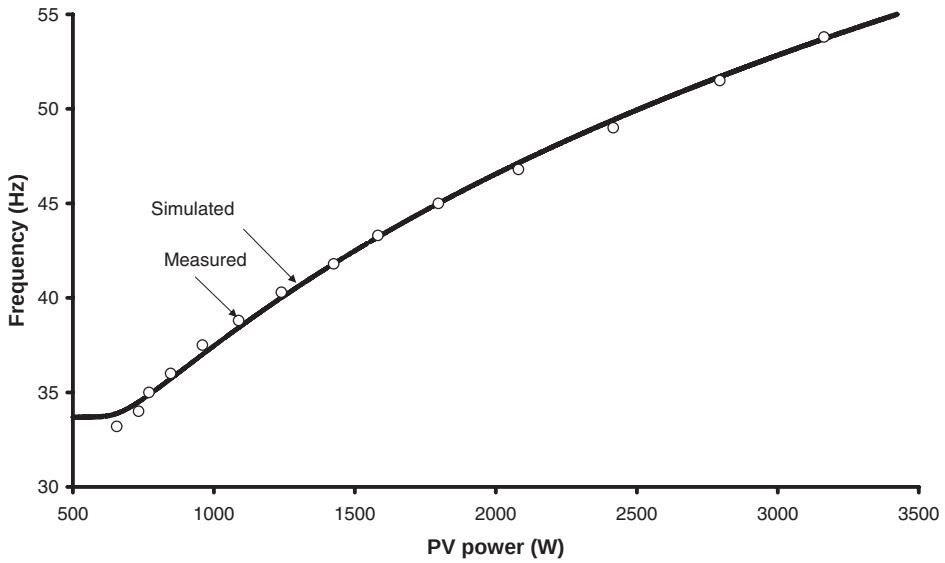

Fig. 10 Simulated and measured laboratory pump frequencies as a function of PV power

an infinite storage capacity algorithm. Moreover, Component Type 103 calculates the potential surplus water and the accumulated surplus water volumes that are not stored in the storage tank also by assuming an infinite storage tank algorithm. Considering a minimum threshold water limit in the tank (given as parameter number 2 in Component Type 103), instantaneous water deficit and accumulated water deficit volumes over any period of operation are calculated by Component Type 103. Component Type 101 determines the unutilized PV array power (P_{NMAX}) when the pump exceeds its maximum speed and the full PV array power (P_{LOSS}) when the storage tank is full and gives them as output numbers 38 and 39, respectively. Component Type 104 Water Desalination Unit uses P_{NMAX} and P_{LOSS} values given from Component Type 101 to predict permeate flowrate, brine flowrate, and other relevant variables.

4 VALIDATION

4.1 System used for validation

Model validation was accomplished through comparison of the simulated results with both the laboratory measurements and long-term field data. The field data were obtained from a system located in Ritem, Jordan (31°6′ N, 36°4′ E), shown in Fig. 5(a), consisting of 90 Siemens Solar mono-crystalline PV modules type M50S with a total peak power of 4.5 $\mathrm{kW_p}$, a 3.5 kVA-DC/AC inverter type Simovert-P-Solar, a

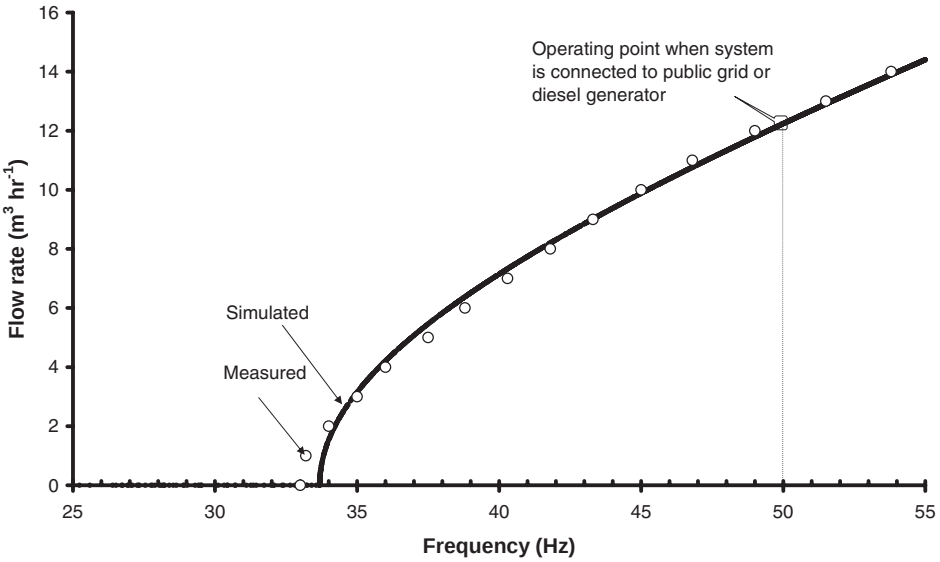

Fig. 11 Simulated and measured laboratory flowrates as a function of pump frequency

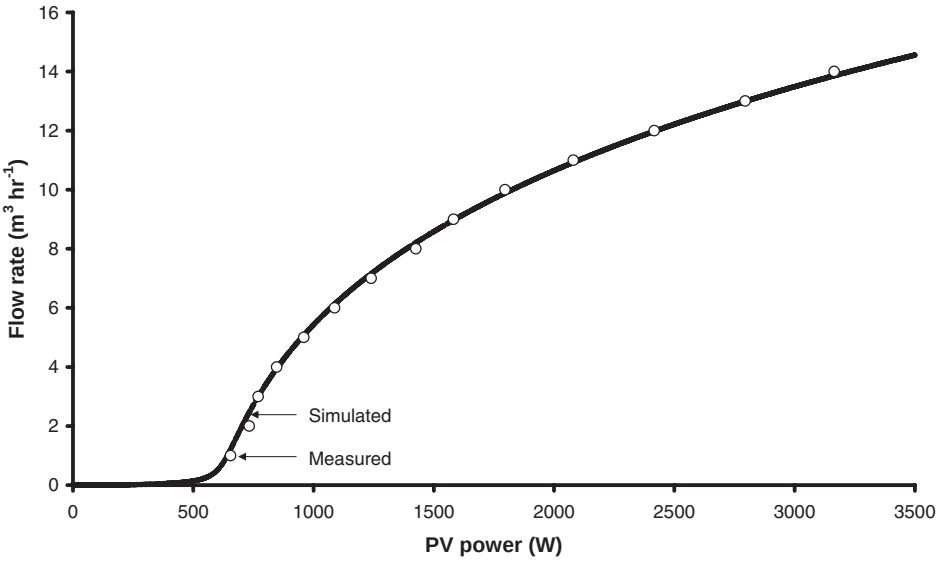

Fig. 12 Simulated and measured laboratory flowrates as a function of PV power

2.2 kW three-phase Franklin induction motor coupled to a centrifugal pump type KSB-UPA 150-3/5, and a 55 m^3 water storage tank (Fig. 5(b)). Figure 5(c) shows the well and the inverter. The total area of the PV array (based on cell area) is 32.4 m^2. PV modules were arranged in five parallel subarrays, each of which contains 18 modules in series. Manufacturers' specifications of the PV modules and the inverter are given in Tables 1 and 2 [**15**, **16**], respectively. The system was installed and operated in a desert area to provide water for nomadic Bedouins and their livestock.

Some components' parameters [**14**] can be determined from either experimental characterization of specific commercial products (e.g. motors) or the use of specialized simulation tools.

4.2 Data handling

Incident insolation, ambient temperature, PV cell temperature, wind speed, PV voltage, PV current, water flowrate, and dynamic water level of the well were measured. The measuring devices used and their approximate errors are listed in Table 3. Measurements taken every 2 s were averaged every 10 min using a data logger and saved. The general specifications of the data loggers are given in Table 4. Specialized software (MODAS12) installed on a laptop computer was used for the following:

(a) setting the data storage interval;
(b) programming the data logger;

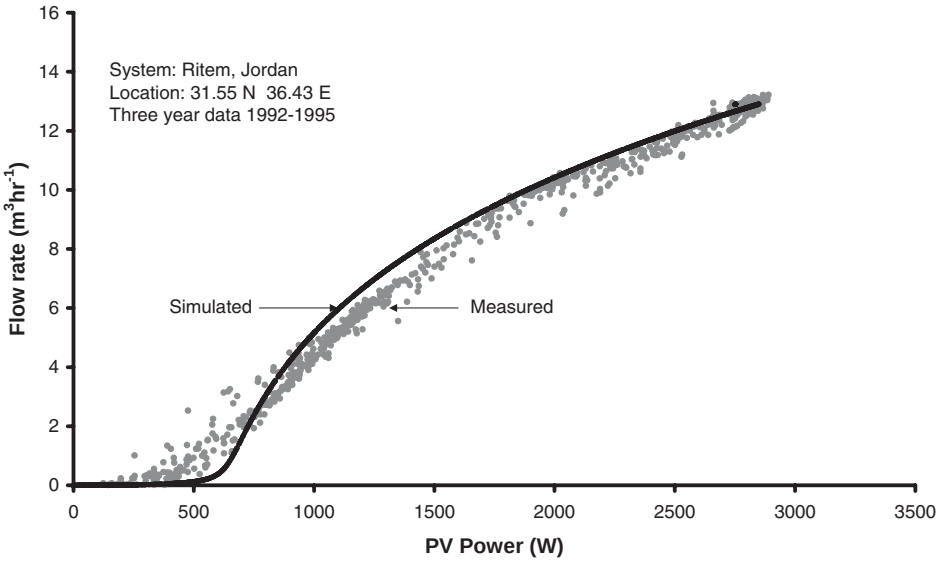

Fig. 13 Simulated and measured field flowrates as a function of their PV powers

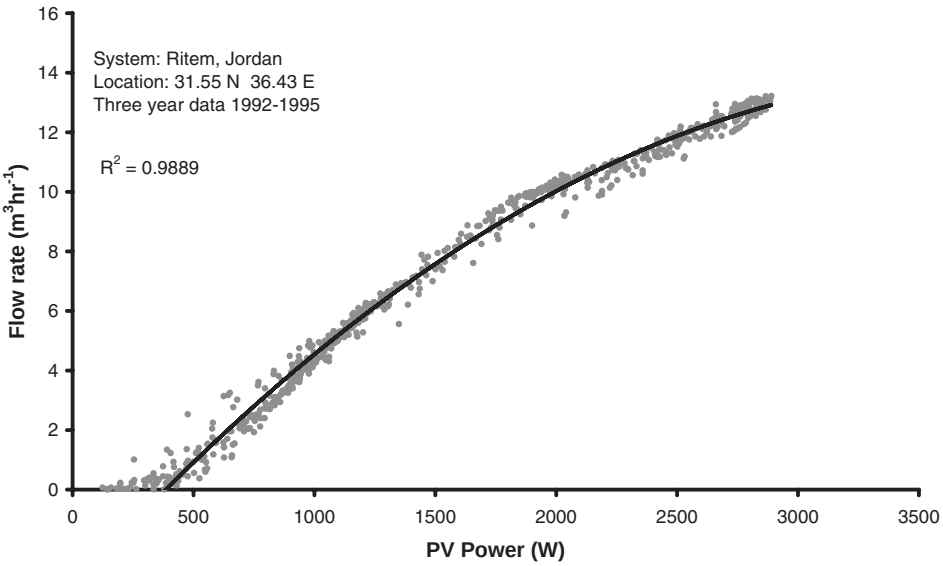

Fig. 14 Measured field flowrate and curve-fitting results as a function of measured PV power

(c) transferring the data from the data logger to the laptop computer;
(d) time-series graphical display of the physical measured data;
(e) production of ASCII-files. The data handling process is summarized in Fig. 6.

4.3 Validation results

The laboratory tests of pumping head as a function of flowrate at 50 Hz frequency were used to generate a complete dataset using a second-order least-square fit, implemented in Component Type 101. Figure 7 shows the measured data points and the generated curve; a good fit can be observed between the measurements and the fitted curve. Data points of pump efficiency as a function of flowrate at 50 Hz frequency are shown in Fig. 8. The measurements were used to generate a complete dataset using least-square fit implemented in Component Type 101. As can be seen in Fig. 8, a good fit can be observed between the measurements and the fitted curve. A regression through measured field data for well system head and flowrate (Fig. 9) gives equation (5)

$$h = h_{\mathrm{st}} + 0.054\,01Q^2 \tag{5}$$

h_{st} was found to be 24 m. h is the total head in metres, which is defined as

$$h = \frac{p_{\mathrm{w}}}{\rho g} \tag{6}$$

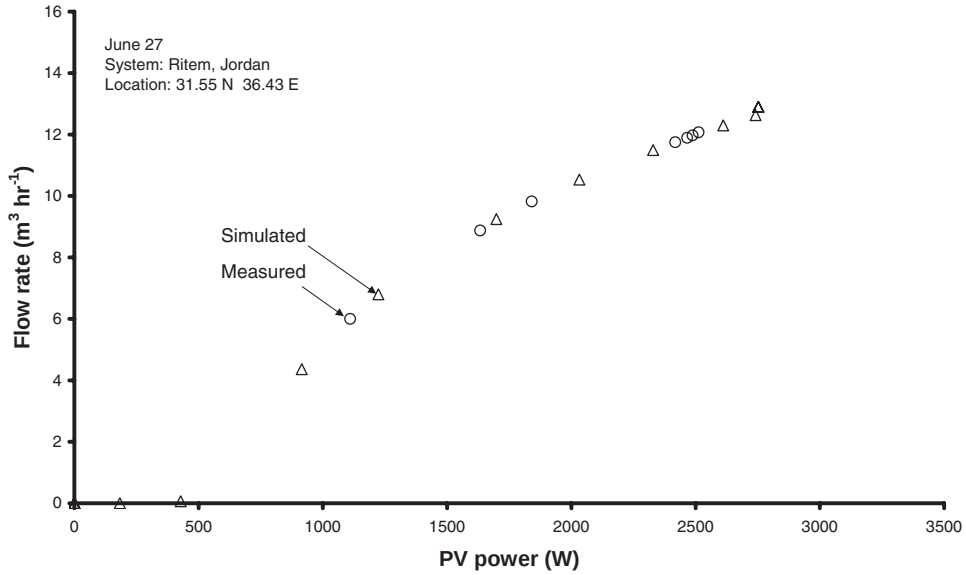

Fig. 15 Simulated and measured field flowrates as a function of measured PV power for a summer day

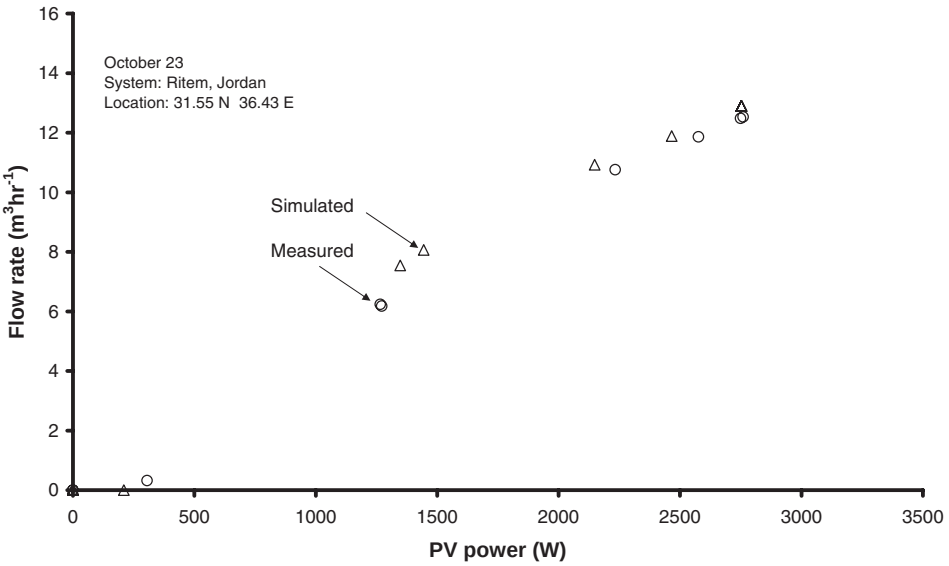

Fig. 16 Simulated and measured field flowrates as a function of measured PV power for a winter day

Figure 10 presents simulated data and laboratory measurements for system frequency as a function of PV power. As can be seen in this figure, the model predicts the system frequency accurately over the most frequent operating range (one-quarter to full load). At low input PV power of less than one-quarter the load, the model overestimates the system frequency by a maximum deviation of 1.5 per cent.

Simulated and measured flowrates as a function of system frequency are shown in Fig. 11. Good agreement is observed over the complete range of operations between measured and simulated flowrates. However, at a zero flowrate, the pump may rotate but the input power is not sufficient to overcome the total pumping head; the water column may rise up to a certain height but not to the surface. Measured and simulated frequencies at which water starts reaching the surface were found to be 33 and 33.7 Hz, respectively, with a 2 per cent deviation. Figure 11 also shows the system operating point if connected to the public grid or a diesel generator where frequency is fixed at 50 Hz approximately. As can be seen in this figure, the model accurately predicts system performance at 50 Hz.

One of the main aims of Component Type 101 is to predict the water output flowrate as a function of the input power. Figure 12 shows simulated data and laboratory measurements of flowrate as a function of PV power. It can be seen that the model predicts laboratory-measured flowrate accurately. Figure 13

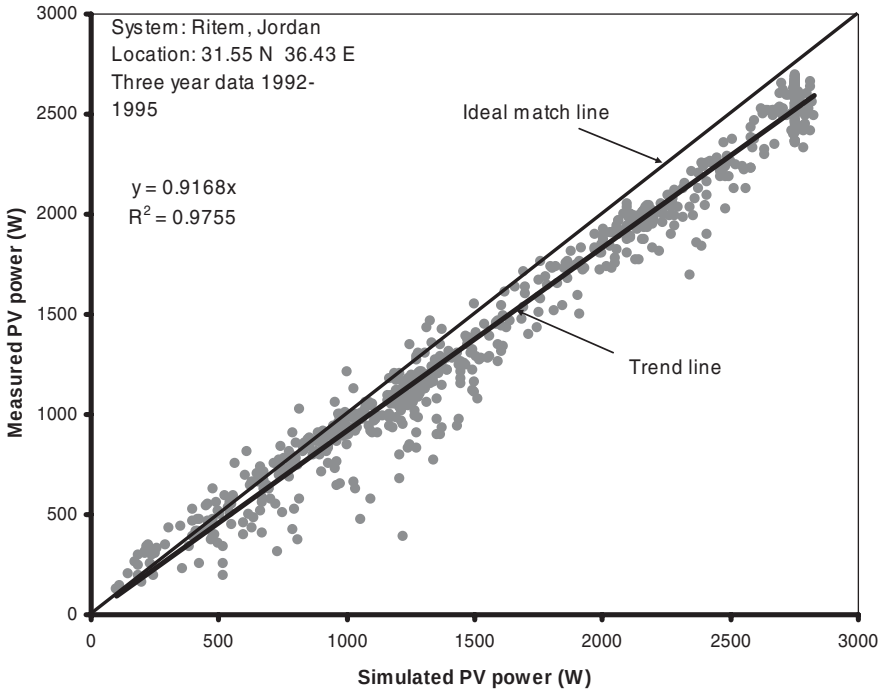

Fig. 17 Comparison between simulated and measured field PV powers

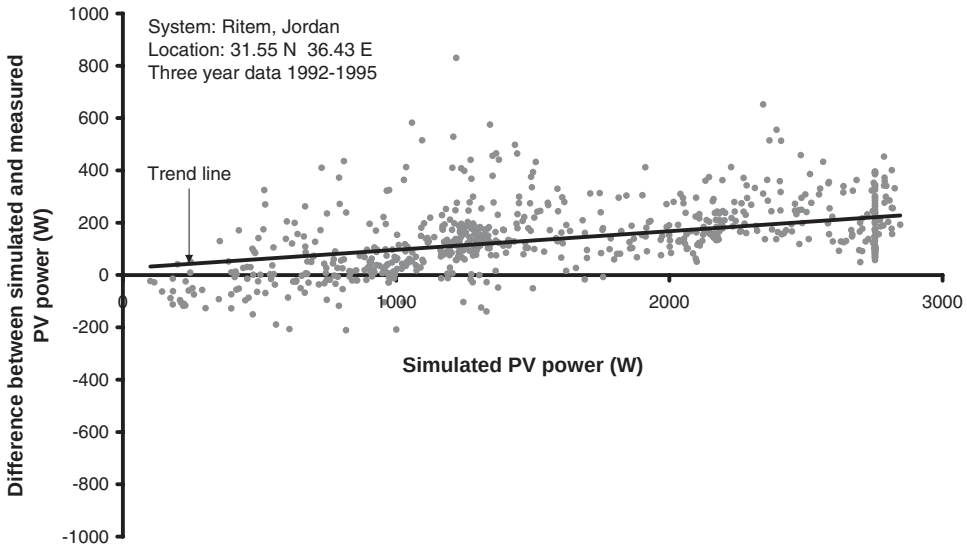

Fig. 18 Difference between simulated and measured PV power versus simulated PV power

shows simulated data and field measurements of flowrate as a function of PV power. Good agreement is attained at high power inputs. However, at low input PV power, deviation between simulated and measured flowrates is observed.

To evaluate the model's accuracy, it is required to compare a complete year of predicted data with a complete year of measured data. However, it is difficult to have continuous operational data for a complete year because the system is turned off when the storage tank is full and thus may give zero flowrates at some sunny periods. To avoid zero data points, available measurements for flowrate as a function of PV power were curve-fitted. The second-order polynomial curve shown in Fig. 14 provided a good fit with an R^2-value of 0.99. For a complete year, the system delivered 35 052 m^3 of water. The model-predicted value was 35 967 m^3. The absolute and relative differences between simulated and measured data are 915 m^3 and 2.6 per cent, respectively. Maximum deviation between predicted and measured data occurs at an input PV power of less than 750 W, which is around one-quarter of the full load power. Data available for values below this power value have been analysed separately, revealing the fact that the accumulated measured water volume is only 0.38 per cent of the

total annual amount and resulting in a negligible error of −0.66 per cent. Figures 15 and 16 compare measured and simulated water flowrates as a function of PV power for representative sample days in summer and winter, respectively.

Figure 17 shows the simulated and measured PV powers over 3 years, with the difference between these simulated and measured values being shown in Fig. 18. For the available measured data, the average difference between simulated and measured PV powers was found to be a 9.4 per cent overestimation. The measured data do not represent the whole 3 years owing to interruptions that occurred when the storage tank being full or the system was turned off. Therefore, interpolations of data were carried out by using curve fitting to provide a complete 3-year dataset. The difference between the simulated data and data with interpolations for a whole year was found to be 5.7 per cent. The latter value would represent a reasonable estimation of the accuracy of the model employed.

5 DEVIATION BETWEEN FIELD MEASUREMENTS AND SIMULATED RESULTS

Variations between measured field data and simulated results may be attributed as follows.

1. Dust deposition on the surface of the PV modules studied in operation under real conditions reduces power output, relative to the type and thickness of dust particles [**17**]. In some cases, PV modules were cleaned whereas in other cases, they were not. Garg [**18**] reported that light transmission was reduced by 30 per cent for glass, owing to dust accumulation, after 30 days of exposure. Nimmo and Seid [**19**] observed degradation of PV efficiency by 40 per cent after 6 months of dust accumulation. El-Shobokshy and Hussein [**20**] concluded that a reduction in the short circuit current by 82 per cent and in the power output by 84 per cent occurred when atmospheric dust particles accumulation reached 250 gm^{-2}.
2. Different types and quantities of dust accumulated on the pyranometer and the PV modules.
3. Mismatch may occur between the shapes of the current–voltage curves of the modules in the array owing to variations in manufacturing [**10**].
4. Static head may vary with time of operation, owing to geological characteristics of the aquifer. This occurs particularly when the water discharge rate is greater than water recharge rate of the well.
5. Spectral and reflection losses in PV modules [**10**].

6 CONCLUSIONS

New TRNSYS models to simulate the water pumping subsystem, the water storage tank, and the water desalination unit were developed. The model has 45 parameters, and 19 inputs were required to achieve satisfactory performance. It has 65 model outputs that allow for comprehensive analysis of the performance of each component. It simulates the following: grid-connected, diesel-powered, and PV-powered water pumping systems; constant voltage tracking, voltage frequency modulation, and maximum power point tracking algorithms; variable inverter frequency with variable motor efficiency, variable inverter frequency with constant motor efficiency, and constant inverter frequency with variable motor efficiency algorithms; and a reverse osmosis water desalination unit that can use the PV power unutilized by the water pumping system.

Models that consider the system to have a constant pumping head can produce erroneous predicted behaviour. The model developed emulates the actual pumping head curve and uses numerical methods to find the intersection working points between the head–flowrate curves of the pump and the well system. For simplicity, manufacturers' performance curves for motors and pumps can be used to obtain data required by the model instead of requiring theoretical motor parameters (as in other models) that are neither available in standard manufacturers' data sheets nor readily obtainable experimentally. Previous models have considered infinite water storage tank capacity. In the actual situation, the tank has finite storage, and it was found, from field data analyses, that this issue is significant in PV water pumping systems applied in remote areas. The model developed during this work considers a storage tank as a component in the system and it calculates water deficit, water surplus, and the unused PV energy by the water pumping systems for each hour and the accumulated values for any concerned period of time. The model also calculates the hourly and the accumulated unused part of the PV energy due to the system reaching its maximum capacity limit.

REFERENCES

1 **Odeh, I., Yohanis, Y. G.,** and **Norton, B.** Economic viability of photovoltaic water pumping systems. *Solar Energy*, 2006, **80**(7), 850–860.
2 **Odeh, I., Yohanis, Y. G.,** and **Norton, B.** Influence of pumping head, insolation and PV array size on PV water pumping system performance. *Solar Energy*, 2006, **80**(1), 51–64.
3 **Tiba, C.** and **Barbosa, E.** Software for designing, simulating or providing diagnosis of photovoltaic water-pumping systems. *Renew. Energy*, 2002, **18**, 191–204.
4 **Abdolzadeh, M., Ameri, M.,** and **Mehrabian, M. A.** The effects of an operating head on the performance of photovoltaic water pumping systems: an experimental investigation. *Proc. IMechE, Part A: J. Power and Energy*, 2009, **223**(A4), 341–347. DOI: 10.1243/09576509JPE693.

5 **Vilela, O. C.** and **Fraidenraich, N.** A methodology for the design of photovoltaic water supply systems. *Prog. Photovolt. Res. Appl.*, 2001, **9**(5), 349–361.

6 **Benghanem, M.** and **Arab, A. H.** Photovoltaic water pumping systems for Algeria. *Desalination*, 2007, **209**(1–3), 50–57.

7 **Martiré, T., Glaize, C., Joubert, C.,** and **Rouvie, B.** A simplified but accurate prevision method for along the sun PV pumping systems. *Solar Energy*, 2008, **82**(11), 1009–1020.

8 **Kaldellis, J. K., Spyropoulos, G. C., Kavadias, K. A.,** and **Koronaki, I. P.** Experimental validation of autonomous PV-based water pumping system optimum sizing. *Renew. Energy*, 2009, **34**(4), 1106–1113.

9 **Hamrouni, N., Jraidi, M.,** and **Chérif, A.** Theoretical and experimental analysis of the behaviour of a photovoltaic pumping system. *Solar Energy*, 2009, **83**(8), 1335–1344.

10 **Fraidenraich, N.** and **Vilela, O. C.** Dynamic behavior of water wells coupled to PV pumping systems. *Prog. Photovolt. Res. Appl.*, 2007, **15**(4), 317–330.

11 **Klein, S. A., *et al.*** *TRNSYS 16, a transient simulation program*, 2006 (Solar Energy Laboratory, University of Wisconsin – Madison, Wisconsin, USA).

12 **Eckstein, J.** *Detailed modeling of photovoltaic system components*. MSc Thesis, Mechanical Engineering, University of Wisconsin – Madison, Wisconsin, USA, 1990.

13 **Odeh, I.** *Modelling, field data analysis and economics of photovoltaic water pumps and the prospects of integrating desalination using reverse osmosis*. PhD Thesis, University of Ulster, 2005.

14 **Odeh, I., Yohanis, Y. G.,** and **Norton, B.** Simulation procedure for the co-optimization of PV water pumping systems. *Proc. IMechE, Part A: J. Power and Energy*, 2010, **224**(A4), 629–640. DOI: 10.1243/09576509JPE844.

15 Siemens Solar. *Simovert P solar instruction manual*, 1996 (Siemens Solar GmbH, Munich, Germany).

16 Siemens Solar. *Solarmodule M 50, Technische Daten*, 1990 (Siemens Solar GmbH, Munich, Germany).

17 **Mondol, J.** *Long-term performance analysis, simulation, optimization and economic analysis of a building integrated photovoltaic system*. PhD Thesis, University of Ulster, UK, 2004.

18 **Garg, H.** Effect of dirt on transparent covers in flat-plate solar energy collectors. *Solar Energy*, 1974, **15**, 299–302.

19 **Nimmo, B.** and **Seid, A.** Effects of dust on the performance of thermal and photovoltaic flat plate collectors in Saudi Arabia: preliminary results. In Proceedings of the 2nd Miami International Conference on *Alternative energy sources*, Miami, Florida, USA, 1979, pp. 223–225.

20 **El-Shobokshy, M.** and **Hussein, F.** Degradation of photo voltaic cell performance due to dust deposition on its surface. *Renew. Energy*, 1993, **3**, 585–590.

APPENDIX

Notation

A_0	zero-order coefficient of the pump head–flowrate curve (m)
A_2	second-order coefficient of the pump head–flow curve (s^2/m^5)
C_4	second-order coefficient of the well system head–flowrate profile (s^2/m^5)
D_W	water deficit flowrate (m^3/h)
$D_{W,A}$	accumulated water deficit (m^3)
E_0	zero-order coefficient of pump efficiency curve (per cent)
E_1	first-order coefficient of pump efficiency curve (per cent s/m^3)
E_2	second-order coefficient of pump efficiency curve (per cent s^2/m^6)
E_3	third-order coefficient of pump efficiency curve (per cent s^3/m^9)
Error	error and/or warning messages (0, 1, 2, 3, 4)
f	frequency (Hz)
F	total friction loss coefficient (s^2/m^5)
g	acceleration due to gravity (m/s^2)
G	in-plane global insolation (same plane of the PV array) (W/m^2)
G_T	total incident insolation on inclined plane (W/m^2)
h, H	total pumping head of the well system and total pressure head of the pump (m), respectively
h_{st}	well static head (m)
L	lowest permitted water storage capacity in tank (m^3)
m_0	zero-order coefficient
m_1	first-order coefficient
m_2	second-order coefficient (W^{-1})
N	pump frequency (Hz)
N_{MAX}	maximum pump frequency (Hz)
P_{HYD}	hydraulic power of the pump (W)
P_{inv}	inverter output power (W)
$P_{INV,R}$	inverter output power when maximum pump frequency is exceeded (W)
P_{LOSS}	unused PV power when storage tank is full and pump is turned off (W)
$P_{LOSS,A}$	accumulated P_{LOSS} (MJ)
$P_{M,G}$	motor output power when electric grid is used (W)
$P_{M,R}$	motor output power when maximum pump frequency is exceeded (W)
P_{MECH}	mechanical motor power used by pump (W)
P_{m-inp}	motor input power (W)
P_{m-out}	motor output power (W)
P_{NMAX}	surplus part of PV power is not used by the system when maximum pump frequency is exceeded (W)
$P_{NMAX,A}$	accumulated P_{NMAX} (MJ)
P_{PV}	PV power (W)
$P_{PV,IN}$	PV power used by inverter (W)
$P_{PV,M}$	maximum PV power (W)
$P_{PV,R}$	PV power when maximum pump frequency is exceeded (W)

$P_{PV,VT}$	PV power at voltage tracking condition (W)
P_{REQ}	power required by the pump to start water delivery to surface (W)
P_w	water pressure (N/m^2)
Q	pump flowrate (m^3/h)
Q_B	brine from both Q_{PLOSS} and Q_{PNMAX} (m^3/h)
Q_{BLOSS}	brine flowrate when P_{LOSS} is used (m^3/h)
Q_{BNMAX}	brine flowrate when P_{NMAX} is used (m^3/h)
Q_{LOSS}	predicted flowrate of discarded water when tank is full (m^3/h)
$Q_{LOSS,A}$	accumulated Q_{LOSS} (m^3)
Q_{OUT}	water flowrate used by the demand side (m^3/h)
Q_P	permeate flowrate from both Q_{PLOSS} and Q_{PNMAX} (m^3/h)
$Q_{P,A}$	accumulated Q_P (m^3)
Q_{PLOSS}	permeate flowrate when P_{LOSS} is used (m^3/h)
$Q_{PLOSS,A}$	accumulated Q_{PLOSS} (m^3)
Q_{PNMAX}	permeate flowrate when P_{NMAX} is used (m^3/h)
$Q_{PNMAX,A}$	accumulated Q_{PNMAX} (m^3)
Q_R	required raw water flowrate to produce Q_{PLOSS} and Q_{PNMAX} (m^3/h)
Q_{RLOSS}	required raw water flowrate when P_{LOSS} is used (m^3/h)
S	storage tank maximum capacity (m^3)
S_W	potential surplus water flowrate when tank is full (m^3/h)
$S_{W,A}$	accumulated surplus water volume (m^3)
T_A	ambient temperature (°C)
T_V	water volume in tank (m^3)
V_0	minimum inverter voltage for inverter equation $V_{inv} = V_0 + V_1 f$ (V)
V_1	first-order coefficient for inverter equation $V_{inv} = V_0 + V_1 f$ (V Hz^{-1})
V_{inv}	inverter voltage (V)
η_{inv}	inverter efficiency (per cent)
η_m	motor efficiency (per cent)
$\eta_{M,R}$	motor efficiency when maximum frequency is exceeded (per cent)
η_p	pump efficiency (per cent)
$\eta_{p,r}$	maximum pump efficiency at rated conditions (per cent)
η_{pv}	operational PV cell efficiency (per cent)
η_{sub}	subsystem efficiency (per cent)
$\eta_{sub,R}$	subsystem efficiency when maximum frequency is exceeded (per cent)
η_{sys}	operational system efficiency (per cent)
$\eta_{sys,R}$	maximum system efficiency considering rating conditions (per cent)
ρ	water density (kg/m^3)